Z^0Z^0 cross section measurement in $ll\nu\overline{\nu}$ decay channel at CDF

CDF note 10358

The CDF Collaboration
URL http://www-cdf.fnal.gov
(Dated: December 13, 2010)

The ZZ cross section measurement is important to test Standard Model predictions of Electro-Weak couplings. Deviations from the expected value can be due to new physics that can contribute through the anomalous trilinear gauge couplings and large extra-dimensions. In addition to that, ZZ events reconstruction is important to set the scale for the $H \rightarrow ZZ$ search.
We aim at the determination of ZZ production cross section and at the reconstruction of a sizeable diboson sample through the $\ell\ell\nu\nu$ decay channel. The analysis that uses 5.9 fb^{-1} of data, starts from dilepton events selection. A Neuro Bayes Neural Network technique is used to discriminate signal from background, after the removal of the Drell Yan events background with a cut on the minimum missing energy. The measured ZZ cross section is $1.45^{+0.60}_{-0.51}$ pb, in agreement with the Standard Model prediction $1.21^{+0.06}_{-0.05}$ pb at Next to Leading Order. This measurement improves the previous CDF combined ZZ production cross section measurement.

PACS numbers:

I. INTRODUCTION

ZZ bosons are expected to be produced with a cross section of $1.21^{+0.06}_{-0.05}$ pb at the Tevatron [1], [2] if only Standard Model (SM) mechanisms contribute to their production. The cross section can be enhanced by new physics phenomena through the anomalous trilinear gauge couplings [3] or large extra-dimensions [4] making the cross section determination a very interesting measurement at the Tevatron. In addition to that, direct ZZ production is an important background for $H \rightarrow ZZ$ searches. For these reasons it is important to reconstruct a ZZ sample as large as possible. In this note we describe the determination of ZZ production cross section exploiting the $\ell\ell\nu\nu$ decay channel with 5.9 fb^{-1} of data that improves the experimental measurement of the cross section. Several ingredients of this analysis are in common with the H→WW analysis [5], the lepton reconstruction and trigger efficiency calculation are the same as well as the *fake* background estimation technique. The major background contribution comes from Drell Yan and it is reduced by cutting on the missing energy projected onto the fully recontructed Z transverse momentum. Then signal and background are separated using a Neural Network technique. The output of the neural Network is fitted taking into account the systematic errors to extract the ZZ cross section.

II. DETECTOR DESCRIPTION

The components of the CDF II detector relevant to this analysis are described briefly here; a more complete description can be found elsewhere [6]. The detector geometry is described by the azimuthal angle ϕ and the pseudo-rapidity $\eta \equiv -\ln(\tan\theta/2)$, where θ is the polar angle of a particle with respect to the proton beam axis (positive z-axis). The pseudo-rapidity of a particle originating from the center of the detector is referred to as $\eta_{\rm det}$.

The trajectories of charged particles are reconstructed using silicon micro-strip detectors [7, 8] and a 96-layer open-cell drift chamber (COT) [9] embedded in a 1.4 T solenoidal magnetic field. For $|\eta_{\rm det}| \leq 1$, a particle traverses all 96 layers of the COT; this decreases to zero at $|\eta_{\rm det}| \approx 2$. The silicon system provides coverage with 6 (7) layers with radii between 2.4 cm and 28 cm for $|\eta_{\rm det}| < 1.0$ ($1.0 < |\eta_{\rm det}| < 2.0$). Outside of the solenoid are electromagnetic (EM) and hadronic (HAD) sampling calorimeters segmented in a projective tower geometry. The first hadronic interaction length (λ) of the calorimeter, corresponding to 19-21 radiation lengths (X_0), uses lead absorber for measuring the electromagnetic component of showers, while the section extending to 4.5-7 λ uses iron to contain the hadronic component. The calorimeters are divided in a central ($|\eta_{\rm det}| < 1$) and forward ($1.1 < |\eta_{\rm det}| < 3.64$) region. Shower maximum detectors (SMX) embedded in the electromagnetic calorimeters at approximately $6X_0$ help in the position measurement and background suppression for electrons. Outside of the central calorimeters are scintillators and drift chambers for identifying muons as minimum ionizing particles. We use three complementary track pattern recognition algorithms which are distinguished by their starting point in COT, silicon, or projection from calorimeter energy cluster to interaction region.

III. LEPTON IDENTIFICATION

In order to maximize signal acceptance and suppress backgrounds from jets and photons misidentified as leptons, we use three (seven) categories of electrons (muons). One additional category, based on central tracks that are not fiducial to calorimeters or muon detectors, is used as either an electron or muon in forming Z^0 candidates. The resulting categories exploit essentially all the tracks and electromagnetic calorimeter clusters available.

All leptons are required to be isolated such that the sum of the E_T for the calorimeter towers in a cone of $\Delta R = \sqrt{(\Delta\eta)^2 + (\Delta\phi)^2} < 0.4$ around the lepton is less than 10% of the electron E_T or muon p_T. The transverse energy E_T of a shower or calorimeter tower is $E\sin\theta$, where E is the associated energy. Similarly, p_T is the component of track momentum transverse to the beam line.

Electron candidates are required to have a ratio of HAD energy to EM energy consistent with originating from an electromagnetic shower and are further divided into two mutually exclusive central categories and one forward category. Both central electron categories require a well-measured COT track satisfying $p_T > 10$ GeV/c that is fiducial to the central SMX and matched to a central EM energy cluster. Candidates for the first central category are also required to have a matching cluster in the shower maximum detector, minimal energy sharing between towers, and a ratio for shower energy E to track momentum of less than $2.5 + 0.0015E_T$. Instead, central category electron candidates are then selected using a likelihood method to combine electron identification variables into one discriminant. A forward electron is required to be fiducial to the forward SMX detector and have energy deposition in both the calorimeter towers and SMX detector consistent with an electron shower shape. For each foward candidate, we also require a matching calorimeter seeded track that is consistent with a standalone reconstructed track formed using hits in the silicon detector to reduce background from photons.

Muons are identified by either a charged track matched to a reconstructed track segment ("stub") in muon chambers or as a stubless minimum ionizing particle fiducial to calorimeters. In addition, stubless muons are required to have at least 0.1 GeV in total calorimeter energy. For $|\eta_{\rm det}| < 1.2$, strict requirements on the number of COT hits and the χ^2 of the track fit are placed on the muon tracks in order to suppress kaon decay-in-flight backgrounds. The category of stubless muons with $|\eta_{\rm det}| > 1.2$ requires that at least 60% of the COT layers crossed by the track have hits. In order to suppress background from cosmic rays, the track's point of closest approach to the beamline must be consistent with originating from the beam.

The final category of leptons is constructed from tracks which are not fiducial to the SMX detectors nor identified as stubbed muons. The requirements for the tracks are the same as stubless muons with $|\eta_{\rm det}| < 1.2$, but without any of the calorimeter requirements. Due to the lack of calorimeter information, electron and muons cannot be reliably differentiated in this region, and this category is therefore treated as having either flavor in the Z^0 candidate reconstruction. If an electron or non-fiducial track candidate is consistent with being due to a photon conversion as indicated by the presence of an additional nearby track, the candidate is vetoed.

To identify the presence of a Z^0 boson decaying to two neutrinos, we use the missing transverse energy $\not\!\!E_T = |\sum_i E_{T,i}\ \hat{n}_{T,i}|$, where the $\hat{n}_{T,i}$ is the transverse component of the unit vector pointing from the interaction point to calorimeter tower i. The $\not\!\!E_T$ is corrected for muons which do not deposit all of their energy in the calorimeter and tracks which point to uninstrumented regions of the calorimeter.

The ZZ candidate events are required to pass one of five online trigger selections implemented in three successively more stringent levels. The final central electron requirement is an EM energy cluster with $E_T > 18$ GeV matched to a track with $p_T > 8$ GeV/c. Muon triggers are based on information from muon chambers matched to a track with $p_T > 18$ GeV/c. The trigger for forward electrons requires an $E_T > 20$ GeV EM energy cluster and an online measurement of the $\not\!\!E_T > 15$ GeV [10]. The trigger efficiencies are determined following the standard CDF procedures [5] using $W \to e\nu$ data for electrons and $Z \to \mu^+\mu^-$ data for muons.

IV. SIGNAL AND BACKGROUND PROCESS SIMULATION

The geometric and kinematic acceptances for the background processes WW, WZ, $W\gamma$, Drell-Yan (DY), $t\bar{t}$, and the ZZ signal process are determined using a Monte Carlo calculation of the collision followed by a GEANT3-based simulation of the CDF II detector [11] response. The Monte Carlo generator used for WW is MC@NLO [12], while for the Drell Yan PYTHIA [13] is used. The WZ, $t\bar{t}$, and the signal process, ZZ have PYTHIA as generator but each cross section has been normalized to the NLO cross section, 0.365 pb for WZ, 0.68778 pb for $t\bar{t}$ and 1.511 pb for ZZ. The $W\gamma$ process is modeled with the generator described in [14]. We use the CTEQ5L parton distribution functions (PDFs) to model the momentum distribution of the initial-state partons [15].

A correction of up to 10% per lepton is applied to the simulation based on measurements of the lepton reconstruction and identification efficiencies in data using Z decays. An additional 10% correction based on $Z \to \ell\ell$ cross section measurements are applied to muons reconstructed from minimum ionizing energy deposits in the forward calorimeter to account for known poor modeling of the track reconstruction in this region.

The resolution of the track momentum in the Monte Carlo is better then in data because the simulation does not take into account the variable data taking conditions of the COT with the time. This does not manifest itself as a difference in the track reconstruction efficiency between data and MC but only as momentum resolution discrepancy. The muon sample is affected by that twice: the dimuon invariant mass resolution of the MC does not reproduce the data and the $\not\!\!E_T$ predicted by the simulation differs from the data. Because both variables are used in the analysis we correct the track curvature for central and forward muons separately in order to improve the agreement between data and MC. Figure 1 shows the comparison data-Monte Carlo for the dimuon sample after the tuning.

The background from W+jets is estimated from a sample of events with an identified lepton and a jet that is required to pass loose isolation requirements and contains a track or an energy cluster similar to those required in the lepton identification. The contribution of each event to the total yield is scaled by the probability that the jet is identified as a lepton. This probability is determined from multijet events collected with a set of jet-based triggers. A correction is applied for the small real lepton contribution using single W and Z boson Monte Carlo simulation.

V. SIGNAL SELECTION

We start the $ZZ \to \ell\ell\nu\nu$ identification by selecting events with two same flavor and opposite sign leptons and small jet activity, 0 or 1 jet at maximum. One of the two leptons must have triggered the event and therefore the transverse momentum (energy) has to be greater 20 GeV/c while for the second lepton the requirement on the minimum p_T is lowered to 10 GeV/c. The two leptons are required to have the invariant mass within ± 15 GeV/c^2 from the nominal

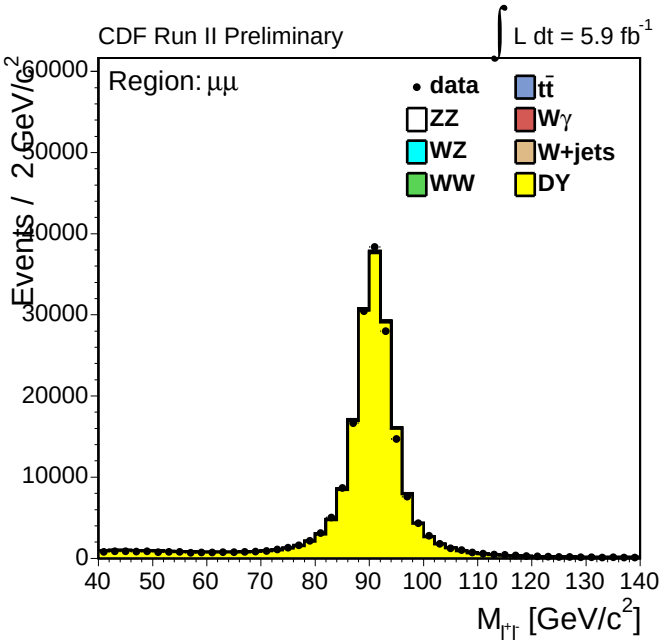

FIG. 1: Invariant mass distribution for dimuon events with 0,1 jet after the track resolution tuning.

Z mass. This event topology is similar to that produced by a single Z boson decaying into two leptons (DY), with unbalanced missing energy. In ZZ events the $\not\!\!E_T$ is due to the two neutrinos coming from the Z decay while in the DY process comes from detector resolution and jets not fully reconstructed. The two neutrinos are reconstructed together as total $\not\!\!E_T$ in the event and since they are almost back-to-back , the amount of $\not\!\!E_T$ is not very large, much less than what we have in events with a single neutrino. To take advantage of that we cut on the $\not\!\!E_T{}^{Ax}$, defined as following. We take the Z boson direction in the transverse plane reconstructed using the two leptons and we project the $\not\!\!E_T$ along, $-\not\!\!E_T{}^{Ax}$, and orthogonal, $\not\!\!E_T{}^{Tr}$, that axis:

$$\not\!\!E_T{}^{Ax} = -\not\!\!E_T \cdot \cos\Delta\phi(\hat{\not\!\!E}_T, \hat{p}_T^Z)$$

$$\not\!\!E_T{}^{Tr} = \not\!\!E_T \cdot \sin\Delta\phi(\hat{\not\!\!E}_T, \hat{p}_T^Z).$$

Figure 2 shows graphically the definition of this variables. In ZZ events the $\not\!\!E_T$ from the two undetected neutrinos

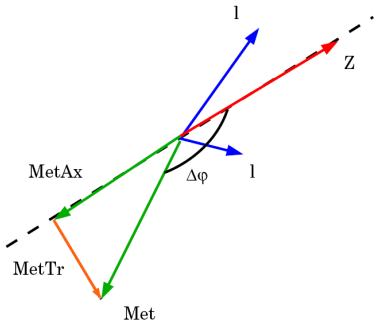

FIG. 2: Schematic draw of the definition of the $\not\!\!E_T$ in the *Axial* and *Transverse* component to the Z axis.

is almost aligned with the reconstructed Z but in the opposite direction. This makes the $\not\!\!E_T{}^{Ax}$ a powerful kinematic variables to distinguish ZZ signal from single Z production also in presence of jets, provided their number is small. The cut $\not\!\!E_T{}^{Ax} \geq 25$ GeV reduces the Drell-Yan background by 99.8% while keeping the ZZ signal untouched.

These cuts are applied to both the muon and electron samples. Due to the additional Monte Carlo tuning performed on the muon sample to have the right track resolution the cuts on the invariant mass and on the $\not\!\!E_T{}^{Ax}$ may have different efficiency on data and MC. A systematic error is evaluated for all the MC samples with muons and tracks but it turned out to be negligeable except for the Dreel Yan Monte Carlo for which an additional error is included in the final systematic uncertainty of the measurement.
To summarize, the ZZ signal is selected requiring:

- Two Opposite Sign and Same Flavor leptons: e, μ or isolated tracks
- One of the leptons has to fire the trigger
- $p_T^1 \geq 20$ GeV/c, $p_T^2 \geq 10$ GeV/c
- $\mathrm{N}_{jets} \leq 1$
- $76 \leq M_{\ell\ell} \leq 106$ GeV/c^2
- $\not\!\!E_T{}^{Ax} \geq 25$ GeV

Table I shows the expected number of events obtained from the MC simulation that pass the above cuts for the processes that contribute to the selected sample compared to the observed number of events.

CDF Run II Preliminary $\int \mathcal{L} = 5.9$ fb^{-1}	
ZZ Signal Region	
$t\bar{t}$	5.8 ± 1.1
DY	881 ± 158
WW	85 ± 8
WZ	35.4 ± 5.0
W+jets	42 ± 11
$W\gamma$	13.9 ± 4.2
Total Background	1113 ± 158
ZZ	49.8 ± 6.3
Data	1162

TABLE I: Expected number of events in 5.9 fb^{-1} for signal and background in the Signal Region, compared with the observed events.

In order to improve the signal to noise ratio we use a multivariate technique which relies on the fact that the MC well describes the signal and the background kinematical variables. The comparison between the Monte Carlo predictions and the data are shown in figure 3 for the variables used in the analysis.

VI. NEURAL NETWORK TRAINING

The NeuroBayes® [16] package, based on a neural network technique, is used to better separate the ZZ events from background. The neural network structure consists of a first layer of input nodes corresponding to event kinematic distributions, an intermediate layer of hidden nodes and one output node. The network is trained using background and signal templates to obtain an output as closest as possible to +1 for signal like events and to -1 for background like events. After the trainig several neural network output templates are created for signal and background predictions that are used to fit the data to extract the ZZ production cross section. Among a variety of kinematic variables we selected those that provide the best signal to background separation, sorted according to NN significance: $\not\!\!E_T$ significance $\not\!\!E_T{}^{Sig}$, transverse $\not\!\!E_T$ projection respect to the momentum of the nearest lepton or jet $\not\!\!E_T{}^{Spec}$, dilepton invariant mass $M_{\ell\ell}$, axial component of the $\not\!\!E_T$ $\not\!\!E_T{}^{Ax}$, dilepton transverse momentum p_T^Z, dilepton opening angles $\Delta\phi(\ell\ell)$ and $\Delta R(\ell\ell)$. Figure 3 shows a comparison between data and Monte Carlo for the variables used in the neural network training. In these plots the ZZ contribution is represented by the white histogram normalized to the expected signal while the red curve ($5\times ZZ$) shows five times the ZZ signal to better appreciate the difference between signal and background.

The result of the neural network training is shown in Fig.4 where the output of the neural network expectations is plotted with the data superimposed in linear (left) and logarithm (right) scale.

It is remarkable that the neural network separates the signal from the dominant background, the Drell Yan, very well. In fact the Drell Yan neural network output peaks at -1 with small contribution under the signal neural network output which is around +1.

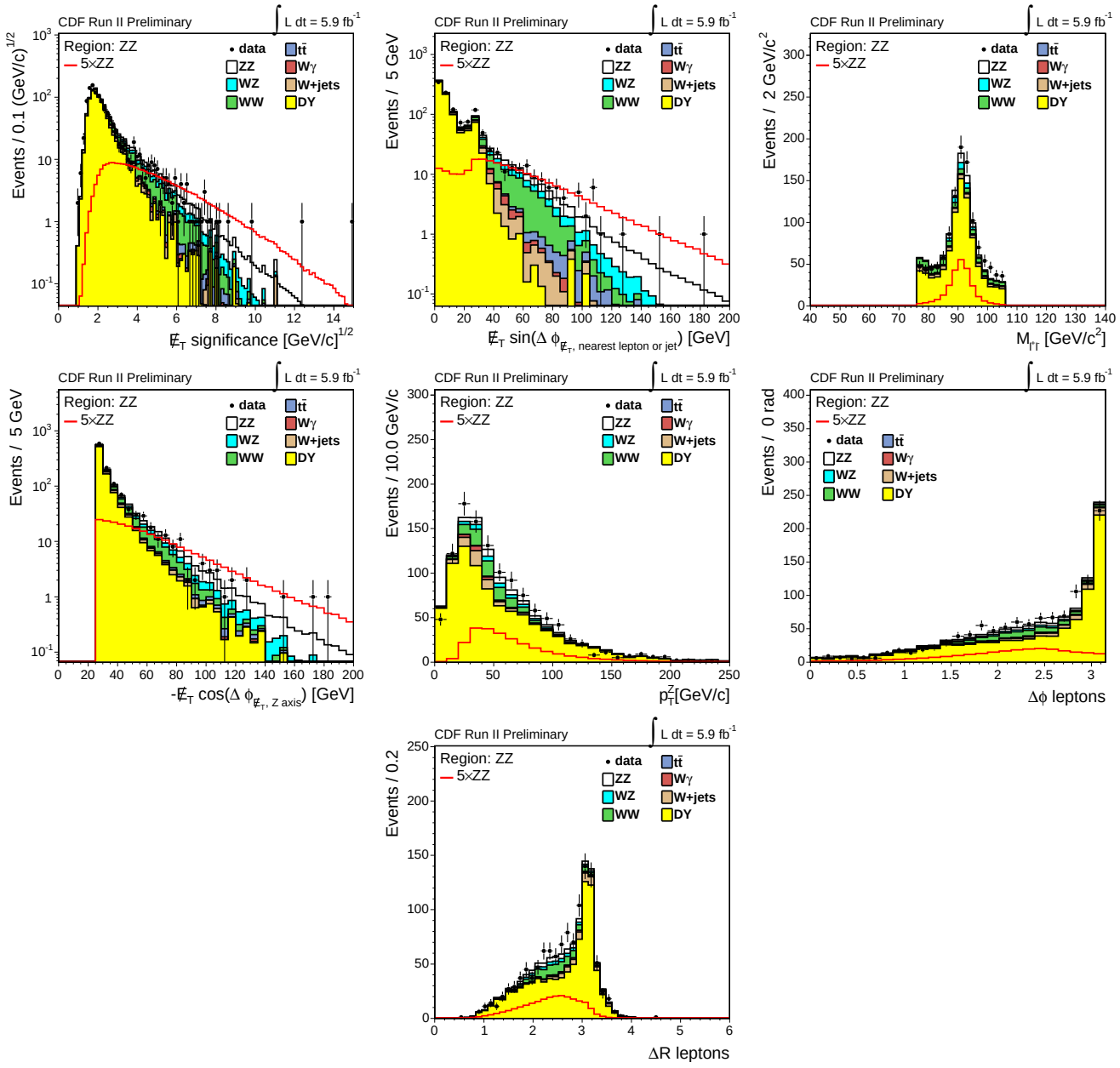

FIG. 3: Kinematic variable distributions for events in the Signal Region, for MC predictions and data. The expected ZZ distribution is represented by the stacked white histogram while the red curve shows five times the expected signal.

VII. MAXIMUM LIKELIHOOD METHOD

A binned maximum likelihood method is used to measure the ZZ production cross section by fitting the data with the Neural Network output distributions of the signal and the background along with their systematics uncertainties.

The likelihood function used is given by the product of the Poisson probabilities for each bin of the Neural Network output with Gaussian constraints to account for the systematic errors, S_c, treated as nuisance parameters. The likelihood is expressed by

$$\mathcal{L} = \left(\prod_i \frac{\mu_i^{n_i} e^{-\mu_i}}{n_i!} \right) \cdot \prod_c e^{-\frac{S_c^2}{2}} \tag{1}$$

where μ_i is the total number of events expected in the i-th bin and n_i is the number of the observed data events in

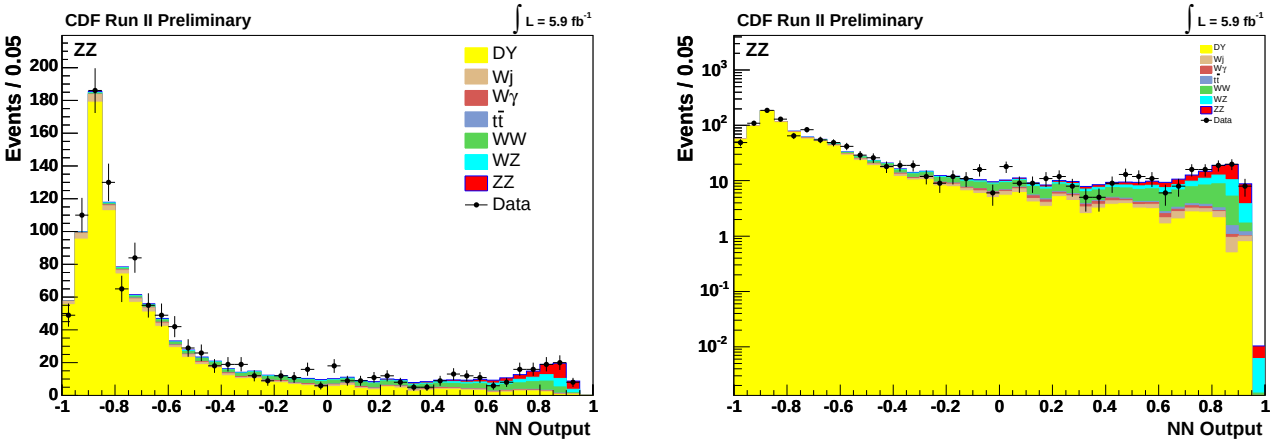

FIG. 4: Left: Neural network output distribution for signal (in red), background expectations with the data (dots)superimposed. Right: same distributions in logarithmic scale.

the i-th bin. μ_i includes also the systematic errors on the expected number of events and is given by the formula:

$$\mu_i = \sum_k \alpha_k \left[\prod_c (1 + f_k^c \cdot S_c) \right] (N_k^{Exp})_i \tag{2}$$

In this expression f_k^c is the fractional uncertainty due to the systematic S_c in the physics process k. $(N_k^{Exp})_i$ is the expected number of events of the physics process k in the i-th bin. This construction of the likelihood function takes into account properly the correlations of the systematic errors. The α_k represents the ratio between the measured cross section and the one used to normalize the Monte Carlo for the process k-th. In the fit the α_k are fixed to one except α_{ZZ} which is the free parameter. The α_{ZZ} returned by the fit multiplied by the input ZZ cross section gives the measured value of the ZZ cross section:

$$\sigma_{ZZ}^{Measured} = \alpha_{ZZ} \cdot \sigma_{ZZ}^{MC} \tag{3}$$

We use the MINUIT program to minimize the negative logarithm of the likelihood and MINOS to extract the asymmetric error on the cross section.

VIII. BACKGROUND MODELING UNCERTAINTIES

Despite the cut on the ${\not\!\!E_T}^{Ax}$ the Drell Yan is still the dominant background. Because the Neural Network separates it from the ZZ signal very well its modeling does not heavily affect the measurement. Since the Monte Carlo simulation may have difficulties to reproduce the Drell Yan integrated cross section and NN output, we validate it with the data. We select events in a kinematic region similar to the one used for the measurement, obtained applying all the signal region cuts but with $15 \leq {\not\!\!E_T}^{Ax} \leq 20$ GeV. The ${\not\!\!E_T}^{Ax}$ cut assures that the Drell Yan in this control region has the same kinematic properties as of the signal region with no overlap with that. The events are processed using the same neural network used for the analysis. We measure the ratio between the data and the SM Drell Yan cross section using the same procedure applied to determine the ZZ cross section. Figure 5 shows on the left the NN output distribution for data in the control region superimposed at the MC expectations and on the right the fit to the data when the Drell Yan fraction is floating. The result of the fit gives a +4.5% discrepancy in the Drell Yan normalization. In order to be conservative we consider ±10% systematic uncertainty on DY cross section which is refereed as *MET modeling* in section IX and table II.

The WW bosons is the dominant background in the Neural Network output distribution in the region where the ZZ signal is located. The WW production is simulated at the Next-to-Leading Order and the agreement between CDF data and MC is very good [17]. Therefore no additional systematic uncertainty is considered for the WW cross section.

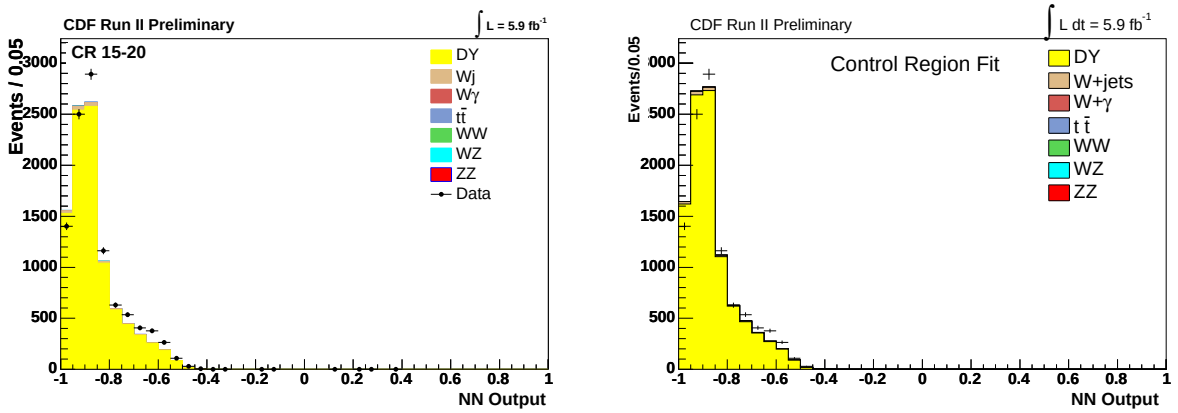

FIG. 5: Left: Neural Network output distribution of data in the control region with the MC expectations obtained using the signal region Neural Network output. Right: Fit of the NN output in the control region. The difference between the two gives the Drell Yan systematic error.

IX. SYSTEMATIC UNCERTAINTIES DETERMINATION

The evaluation of the systematic errors on the measurement is done following the same procedure used in the $H \to WW$ analysis, a detailed description can be found here [5]. The results of the procedure applied to the ZZ production cross section determination are summarized in table II and briefly described below.

Source	ZZ	WW	WZ	$t\bar{t}$	DY	Wγ	W+jets
Cross Section		6%	6%	10%	5%	10%	
MC-run dep.				10%			
PDF	2.7%	1.9%	2.7%	2.1%	4.1%	2.2%	
NLO	10%		10%	10%		10%	
$\mathcal{L}$	5.9%	5.9%	5.9%	5.9%	5.9%	5.9%	
Conversion						10%	
Jet Modeling	2%		2.8%		7.3%	4%	
Fakes							26.6
Lepton ID Eff.	3%	3%	3%	3%	3%		
Trigger Eff.	2%	2%	2%	2%			
$\not\!\!E_T$ modeling					10%		
$\not\!\!E_T^{Ax}$ cut					30%*		

*Only for dimuon sample.

TABLE II: Contribution of different sources to the systematics uncertainties on the acceptance of signal and background.

Uncertainties originating from lepton selection and trigger efficiency measurements are obtained varying the efficiency within their uncertainty and propagating it through the acceptance calculation. This gives uncertainties typically around 3% for the lepton identification and 3% for the trigger efficiency for signal and background processes.

The Monte Carlo used are at the LO and the error on the acceptance due to potential contributions of higher-order effects are evaluated for all the samples except the WW that is simulated at Next-to-Leading order. The uncertainty is taken as the difference between the acceptance at leading order and at next-to-leading order for the WW which is 10%.

The variation of the jet energy scale up and down by one standard deviation determines the systematic error due to the jet modeling.

The MC sample are generated taking into account different run conditions and luminosity weighted according to each different time period. The $t\bar{t}$ Monte Carlo sample currently does not cover the entire data run range and we add an additional uncertainty on the acceptance for that.

The acceptance variations due to PDF model uncertainties is taken as the maximal acceptance variation obtained using the 20 pairs of PDF sets described in [18].

The $W\gamma$ background contribution has an additional uncertainty of 10% due to the detector material description in the MC and conversion veto efficiency.

The systematic uncertainty on the W+jets background contribution is determined as the differences in the measured probability that a jet is identified as a lepton for jets collected using different jet E_T trigger thresholds. These variations correspond to changing the parton composition of the jets and the relative amount of contamination from real leptons.

The uncertainties on the WW/WZ and $t\bar{t}$ theoretical cross sections are assigned to be 6% [19] and 10% [20, 21], respectively. In addition, signal and background predictions obtained from simulation have an additional 5.9% uncertainty originating from the luminosity measurement [22].

The Drell-Yan modeling has additiona sistematic errors. We assign a $\pm 10\%$ uncertainty on the cross section normalizzation evaluated in the control region as described in Section VIII and referred in table II as *MET modeling*. Another systematic error of $\pm 30\%$ affects the dimuon DY sample, due to the uncertainty on the invariant mass and ${\not\!\!E}_T^{\prime\,Ax}$ cut acceptance (see Sec. V).

X. RESULTS

The fit to the neural network output distribution of the data gives a ZZ production cross section of

$$\sigma(p\overline{p} \rightarrow ZZ) \;=\; 1.45^{+0.45}_{-0.42}(stat.)^{+0.41}_{-0.30}(syst.)\ \text{pb} \tag{4}$$

that corresponds, if we combine statistical and systematic uncertainty, to

$$\sigma(p\overline{p} \rightarrow ZZ) \;=\; 1.45^{+0.60}_{-0.51}\ \text{pb}. \tag{5}$$

This measurement compares very well with the latest theoretical prediction [1], [2] of

$$\sigma(ZZ) \;=\; 1.21^{+0.05}_{-0.04}(scale)^{+0.04}_{-0.03}(PDF)\ \text{pb}.$$

Figure 6 shows the fit result with the ZZ signal in red.

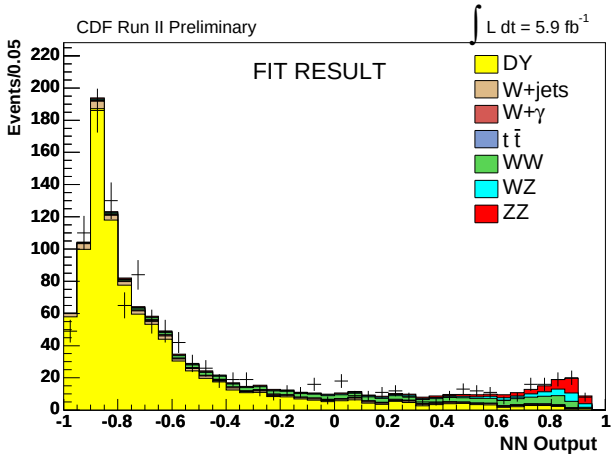

FIG. 6: Result of the fit to the data. The ZZ signal stacked in red over the other physics process. The signal plus background predictions are given by the blue dashed line.

The significance of the measurement is evaluated with a Frequentist approach generating 200k pseudo-experiments. The test-statistic used is defined as:

$$t_s = (-2\ ln\mathcal{L}_{ZZ\ free}) - (-2\ ln\mathcal{L}_{null\ hp}) \tag{6}$$

where the $\mathcal{L}_{ZZ\ free}$ is the best fit likelihood with the ZZ contribution floating and $\mathcal{L}_{null\ hp}$ is the best fit likelihood in the *only-background* hypothesis. From the pseudo-experiments we found a p-value of $(3.35 \pm 0.04)\cdot 10^{-2}$, corresponding to a significance of 2.1 σ.

XI. CONCLUSIONS

The ZZ production cross section has been measured selecting ZZ events through the decay channel $ZZ \rightarrow ll\nu\nu$ using 5.9 fb^{-1} of data. The analysis uses the extended leptons selections and a Neural Network technique to discriminate signal from background. The ZZ cross section is obtained by fitting the Neural Network output as a sum of MC

template distributions of the contributing physics process and constructing a binned likelihood for each bin of the Neural Network output. Gaussian terms in the likelihood are used to constrain the systematic errors within their estimated uncertainties. The fit results gives a production cross section $\sigma(p\overline{p} \to ZZ) = 1.45^{+0.45}_{-0.42}(stat.)^{+0.41}_{-0.30}(syst.)$ pb, in agreement with the theoretical prediction. This measurement improves the previous CDF published measurement of the ZZ cross section [23], obtained by combining the $\ell\ell\ell'\ell'$ and $\ell\ell\nu\nu$ channel, with 1.9 fb^{-1}.

[1] J. Campbell and R. K. Ellis, Phys. Rev. **D60**, 113006 (1999).
[2] J. Campbell and R. K. Ellis, *MCFM - Monte Carlo for FeMtobarn processes* (2010), We ran MCFM Monte Carlo with the MSTW2008 PDF set and varying the factorizzation and renormalizzation scale.
[3] K. Hagiwara, R. D. Peccei, D. Zeppenfeld, and K. Hikasa, Nuclear Physics B **282**, 253 (1987), ISSN 0550-3213.
[4] M. Kober, B. Koch, and M. Bleicher, Phys. Rev. **D76**, 125001 (2007), 0708.2368.
[5] CDF Collaboration, *Inclusive Search for Standard Model Higgs Production in the WW Decay Channel Using the CDFII Detector* (2010), Phys. Rev. Lett. 104.
[6] R. Blair, *et al.* (CDF Collaboration) (1996), FERMILAB-PUB-96/390-E.
[7] A. Sill *et al.*, Nucl. Instrum. Methods A **447**, 1 (2000).
[8] A. Affolder *et al.*, Nucl. Instrum. Methods A **453**, 84 (2000).
[9] T. Affolder *et al.*, Nucl. Instrum. Methods A **526**, 249 (2004).
[10] K. Hagiwara, S. Ishihara, R. Szalapski, and D. Zeppenfeld, Phys. Rev. D **48**, 2182 (1993).
[11] R. Brun, R. Hagelberg, M. Hansroul, and J. Lassalle, CERN-DD-78-2-REV and CERN-DD-78-2.
[12] S. Frixione and B. R. Webber, JHEP **06** (2002), hep-ph/0204244.
[13] T. Sjostrand, S. Mrenna, and P. Skands, JHEP **05**, 026 (2006).
[14] U. Baur and E. L. Berger, Phys. Rev. **D47**, 4889 (1993).
[15] H. L. Lai *et al.* (CTEQ), Eur. Phys. J. **C12**, 375 (2000).
[16] M. Feindtz and U. Kerzel, Nucl. Instr. Meth. **A**, 190 (2006).
[17] CDF Collaboration, *Measurement of the W+W- Production Cross Section and Search for Anomalous WWg and WWZ Couplings* (2010), Phys. Rev. Lett. 104.
[18] S. Kretzer, H. L. Lai, F. I. Olness, and W. K. Tung, Phys. Rev. **D69**, 114005 (2004).
[19] J. M. Campbell and R. K. Ellis, Phys. Rev. **D60**, 113006 (1999).
[20] N. Kidonakis and R. Vogt, Phys. Rev. **D68**, 114014 (2003).
[21] M. Cacciari, S. Frixione, M. L. Mangano, P. Nason, and G. Ridolfi, JHEP **04**, 068 (2004).
[22] D. Acosta *et al.*, Nucl. Instrum. Meth. **A494**, 57 (2002).
[23] CDF Collaboration, *Strong Evidence for ZZ production in $p\bar{p}$ Collisions at $\sqrt{s}$= 1.96 TeV* (2008), Phys. Rev. Lett. 100.